

Numerical calculation of the NO formation in a multi-point combustion chamber and results of the associated validation experiments

Lionel Matuszewski[†], Francis Dupoirieux^{†1}, Christian Guin[†], Frédéric Grisch[‡]

[†]*Fundamental and Applied Energetics Department (DEFA)*

[‡]*Physics, Instrumentation and Sensing (DMPH)*

Office National d'Études et de Recherches Aérospatiales

Chemin de la Hunière, 91761 Palaiseau Cedex, France

Abstract: This paper presents some numerical simulations of a multi-point combustion chamber including the calculation of the NO formation by a lagrangian method well adapted to take into account the turbulence-chemistry interaction. The simplifying assumption of axial symmetry was used to limit the computation time and made it possible to obtain numerically the influence of a geometrical parameter, the direction of the main inlet air flow, on the NO emission index. The main features of the calculated reactive flows are in agreement with the experimental visualizations but the NO emission index which is numerically obtained is higher than the measured one. The cause of this discrepancy is probably that the radiative transfer was not taken into account in the simulations.

Keywords: multi-point combustor, pollutant formation, NOx emission, turbulent combustion, lagrangian combustion model.

Nomenclature

r	radial coordinate
D_k	diffusion coefficient of the k^{th} species
k	turbulent kinetic energy
P	composition PDF
p	pressure
r	radial coordinate
t	time
u	axial component of the gas velocity
v	radial component of the gas velocity
w	azimuthal component of the gas velocity
\mathbf{v}	velocity vector of the gas
\mathbf{v}_p	droplet velocity vector
x	axial coordinate

Greek symbols

ε	dissipation rate of the turbulent kinetic energy
λ	gas conductivity
μ	gas viscosity
Φ	diffusion flux vector of component Φ (laminar and turbulent diffusion)
ρ	density
Ψ	composition vector
ω	reaction source term

¹Corresponding author, Email: francis.dupoirieux@onera.fr, Tel: 33 1 69936042

Subscripts

- g refers to the gas
- p refers to the liquid droplets (particles)

Superscripts

- $\overline{(\quad)}$ Reynolds average
- $\widetilde{(\quad)}$ Favre average
- $(\quad)''$ Favre fluctuation

1 Introduction

The improvement of the thermodynamic efficiency of aircraft engines leads to higher temperatures and pressures in combustion chambers. This evolution increases the tendency of the engines to produce NOx. To comply with more and more stringent standards for pollutant emissions new designs of combustion chambers are required. The first idea was to create Dual Annular Combustor (DAC) [1, 2, 3] including two injections heads, one dedicated to high power operating conditions, the other dedicated to idle or low power operating conditions. The first injection head is designed to give a small residence time to the burnt gas, the second one to ensure a stable combustion. Despite better performance in terms of NOx emissions DAC combustors can not be considered as a totally satisfactory solution because the temperature profile in the outlet section of the combustor is not homogeneous. The research has therefore been focused on other concepts like LPP [4, 5] or RQL [6, 7] combustors. With the LPP combustor other difficulties arise: at idle or low power operating conditions the combustion is not stable and extinction or flame instabilities can occur; moreover flashback in the premixing pipe is possible. RQL combustors are free from these difficulties but the existence of a zone with a very high Fuel-Air Ratio (FAR) can lead to large concentrations of CO, unburned hydrocarbons and soot particles. The oxidation of these pollutants in the lean part of the burner can be difficult. To overcome these obstacles a new idea consisting in bringing close to each other the pilot zone and the low FAR combustion zone has taken shape through the Twin Annular Premixing Swirling (TAPS) or multipoint combustor [8, 9], in other words fuel injection through multiple points around or within an air flow undergoing a strong swirl. This concept initially developed by GE is now widely studied, in particular in Europe through EEC research programmes as NEWAC (New Aero Engine Core Concept), Intellect D.M. (Integrated Lean Low-Emission Combustor Design Methodology) or TLC (Towards Lean Combustion).

The optimization of these new concepts requires experiments reproducing the real operating conditions associated with accurate and reliable measurements but the design is now greatly facilitated by the numerical simulation of reactive flows [3, 10, 11]. The unsteady simulation of the large turbulent structures of the flow is now possible for industrial burners [12, 13, 14] but the computation time of such simulations is too large to make possible an exploration of the influence of geometrical or physical parameters over a wide range of variation. In this paper we describe the numerical simulations giving the influence a geometrical parameter of the injector, the gyration angle of the injection swirl, on the nitrous oxide production of a multi-point injector. These RANS simulations are based on a mixed eulerian-lagrangian method well suited to give access to the concentration of minor species [15, 16, 17, 18]. Since the important phenomena are located around the axis of the injector, the combustor has been calculated considering a 2D axisymmetric geometry. This simplifying assumption makes possible the realization of a large number of calculations. Before giving the results of this parametric study, the main features of the

calculated reactive flows are discussed and compared to available experimental PLIF visualizations [19].

2 Numerical method and physical models

The aim of our numerical simulations is to obtain the variations of the NOx emission index of a multi-point combustor as function of the gyration angle of the air flow in the swirlers of the fuel injector. This implies the use of a combustion model able to describe correctly the interaction between turbulence and chemistry. As mentioned above our simulations are based on a method [20] which associates the eulerian resolution of the usual balance equations of mass, momentum and energy with the lagrangian resolution of a species PDF transport equation. This kind of method is very efficient for the calculation of pollutant concentrations in turbulent reactive flows. Because of the large number of calculations to be done it was necessary to limit the computation time of the eulerian part. Therefore the geometry was considered as 2D axisymmetric although the external walls located far from the injector axis are not cylindrical. The real external walls were replaced by a cylindrical fictitious wall keeping the real section of the combustor. Despite the 2D calculation grid one balance equation for each of the three velocity component (axial, radial and azimuthal) has to be solved.

In addition to the eulerian balance equations which apply to the gas phase an additional model must be introduced to treat the liquid fuel which creates a dispersed phase in interaction with the gaseous mixing. A lagrangian method has also been chosen for the tracking of the fuel droplets. The interaction between the liquid phase and the gas phase are taken into account through source terms in the eulerian balance equations of the gas. These source terms account for all the phenomena related to the vaporization of the fuel.

2.1 The eulerian balance equations

For the gas phase the following Partial Differential Equations are solved:

- axial velocity component

$$\frac{\partial \bar{\rho} \tilde{u} r}{\partial t} + \frac{\partial (\bar{\rho} \tilde{u}^2 + \bar{\Phi}_x^u + \bar{p}) r}{\partial x} + \frac{\partial (\bar{\rho} \tilde{u} \tilde{v} + \bar{\Phi}_r^u) r}{\partial r} = 0, \quad (1)$$

- radial velocity component

$$\frac{\partial \bar{\rho} \tilde{v} r}{\partial t} + \frac{\partial (\bar{\rho} \tilde{u} \tilde{v} + \bar{\Phi}_x^v) r}{\partial x} + \frac{\partial (\bar{\rho} \tilde{v}^2 + \bar{\Phi}_r^v) r}{\partial r} = -r \frac{\partial \bar{p}}{\partial r} + \bar{\rho} (\tilde{w}^2 + \widetilde{w''^2}), \quad (2)$$

- azimuthal velocity component

$$\frac{\partial \bar{\rho} \tilde{w} r}{\partial t} + \frac{\partial (\bar{\rho} \tilde{u} \tilde{w} + \bar{\Phi}_x^w) r}{\partial x} + \frac{\partial (\bar{\rho} \tilde{v} \tilde{w} + \bar{\Phi}_r^w) r}{\partial r} = -\bar{\rho} (\tilde{v} \tilde{w} + \widetilde{v'' w''}), \quad (3)$$

- scalar quantities

$$\frac{\partial \bar{\rho} \tilde{f} r}{\partial t} + \frac{\partial (\bar{\rho} \tilde{u} \tilde{f} + \bar{\Phi}_x^f) r}{\partial x} + \frac{\partial (\bar{\rho} \tilde{v} \tilde{f} + \bar{\Phi}_r^f) r}{\partial r} = S_f r, \quad (4)$$

where f stands for the scalar quantities, i. e. the mass fractions, the enthalpy and the turbulent

quantities k and L . The source term S_f accounts for the chemical reactions, the fuel vaporization, the creation and the dissipation of the turbulent quantities. If f is the enthalpy, S_f contains in addition the term $\frac{\partial \bar{p}}{\partial t}$.

These PDE are Favre averaged and the turbulence is taken into account through a two equations k-L model with source terms adapted to variable density flows. Since the eulerian step is followed by a lagrangian calculation including a rather accurate chemistry, the simple Magnussen model [21] is used to estimate the averaged reaction source terms. This model received however the following improvement: An ignition temperature was introduced in the calculation of the source terms in order to prevent the flow from non physical ignition in the immediate wake of the fuel injector.

The PDE are integrated in time by the solver CHARME of the CEDRE code [22] using a time implicit method and are solved until convergence, i. e. until the terms $\frac{\partial}{\partial t}$ vanish.

2.2 The lagrangian treatment of the liquid phase

The solver SPARTE of the CEDRE code is used to calculate the trajectory, the secondary fragmentation and the vaporization rate of the fuel droplets. For the trajectory calculation only the drag force is considered. The expression of this drag force is

$$\mathbf{F}_d = \frac{1}{2} \pi \rho r_p^2 C_d \|\tilde{\mathbf{v}} + \mathbf{v}'' - \mathbf{v}_p\| (\tilde{\mathbf{v}} + \mathbf{v}'' - \mathbf{v}_p), \quad (5)$$

where r_p is the droplet radius, C_d is the drag coefficient, \mathbf{v}'' is a gas velocity fluctuation which accounts for the turbulent dispersion of the droplets and \mathbf{v}_p is the velocity of the droplets. The drag coefficient is given by

$$C_d = \begin{cases} \frac{24}{Re_p} (1 + 0.15 Re_p^{0.687}) & \text{if } Re_p \leq 1000 \\ 0.445 & \text{if } Re_p > 1000 \end{cases}. \quad (6)$$

The gas velocity fluctuation \mathbf{v}'' is calculated from a Wiener process by resolution of the following differential equation

$$d\mathbf{v}'' = -\frac{\mathbf{v}''}{\tau_g} dt + \sqrt{\frac{4k}{3\tau_g}} dW_t, \quad (7)$$

where τ_g is a lagrangian correlation time for the gas which is estimated from the turbulent quantities and W_t is a stochastic Wiener process.

A secondary fragmentation happens when the droplet Weber number becomes higher than a critical value considered equal to 12. The size distribution of the secondary smaller droplets is assumed exponential.

The vaporization rate of the droplets is deduced from the well known d^2 -law

$$\frac{d d_p^2}{dt} = -K_{vap}, \quad (8)$$

where d_p is the droplet diameter and K_{vap} is given by

$$K_{vap} = \frac{4\mu}{\rho_p} \frac{Sh}{Sc} \ln(1 + B_m). \quad (9)$$

ρ_p is the density of the liquid fuel, Sc is the Schmidt number of the surrounding gas, Sh is the Sherwood number of the gas-droplet interaction and B_m is the Spalding mass number estimated

as follows

$$B_m = \frac{y_s - y_g}{1 - y_s}, \quad (10)$$

where y_s and y_g are the fuel mass fractions on the droplet surface and in the surrounding gas far from the droplet surface, respectively; y_s is calculated from the saturation vapor pressure as a function of the liquid fuel temperature. Sh is calculated as follows using a Ranz-Marshall correlation and the previous estimation of B_m

$$Sh = (2 + 0.57 Re_p^{\frac{1}{2}} Sc^{\frac{1}{3}}) \frac{\ln(1 + B_m)}{B_m}. \quad (11)$$

The temperature T_p of the liquid fuel which is required for the estimation of y_s is obtained using the following energy balance for the droplets

$$m_p c_{p_p} \frac{dT_p}{dt} = \pi Nu \lambda_g d_p (T_g - T_p) + \frac{dm_p}{dt} L_v(T_p), \quad (12)$$

where m_p is the mass of the droplet, c_{p_p} is the heat capacity of the liquid fuel, Nu is the Nusselt number of the gas-droplet interaction, λ_g is the gas conductivity and L_v is the fuel latent heat of vaporization. Nu is estimated by a correlation similar to that of Eq. [11], except that the Spalding mass number B_m is replaced by the Spalding temperature number B_T .

2.3 Lagrangian resolution of the composition PDF equation

The transport equation of the composition PDF $\tilde{P}(\Psi)$ where Ψ is the composition vector can be written

$$\frac{\partial \tilde{\rho} \tilde{P}}{\partial t} + \frac{\partial}{\partial x_j} [\tilde{\rho} \langle v_j | \Psi \rangle \tilde{P}] + \frac{\partial}{\partial \psi_k} [\tilde{\rho} \omega_k \tilde{P}] + \frac{\partial}{\partial \psi_k} \left[\tilde{\rho} \left\langle \frac{\partial}{\partial x_j} \left(D_k \frac{\partial Y_k}{\partial x_j} \right) \middle| \Psi \right\rangle \tilde{P} \right] = 0. \quad (13)$$

The components ψ_k of the vector Ψ include both the species mass fractions and the enthalpy variable. Because of its large number of degrees of freedom this equation is generally solved using a particle tracking method. It consists in the resolution of ordinary differential equations which give the time evolution of the composition of fluid pockets representing the gas flow, i. e. the trajectory of particles in the composition space (or phase space). Knowing these trajectories it is easy to deduce the distribution of the particles in the phase space and thus to obtain the PDF \tilde{P} or to calculate any interesting mean quantity. The time evolution equations of the particles can be written as follows

$$\frac{d}{dt} \begin{pmatrix} \mathbf{Y} \\ \mathbf{x} \end{pmatrix} = \begin{pmatrix} \Xi + \omega \\ \mathbf{v} + \mathbf{v}'' \end{pmatrix}, \quad (14)$$

where \mathbf{Y} is the composition vector, i. e. the position of the particle in the phase space, \mathbf{x} is the position of the particle in the physical space, \mathbf{v} is the average velocity of the particle, \mathbf{v}'' is the velocity fluctuation of the particle, ω is the vector of the reaction source terms and Ξ is a stochastic vector which accounts for the mixing at small scales between the gas pockets and the surrounding fluid. In practice the pockets of fluid are injected on the boundaries in all the inlet sections and inside the combustor in all the cells of the calculation grid where the liquid fuel droplets vaporize. The injection rate of the fluid pockets is proportional to the local rate of gas injected or released by vaporization. After the tracking of all the particles, the mean concentration of the pollutant in a given cell of the calculation grid can be obtained by averaging on all the fluid pockets which crossed the cell.

Reaction	A [$m^3/(mol\ s)$]	b	E_a [kJ/mol]
R1	9×10^7	0	313
R2	6.3×10^3	1	26
R3	1×10^6	0	0

Table 1: Chemical constants for thermal NO

To comply with Eq. [13], the components Ξ_k of Ξ must satisfy

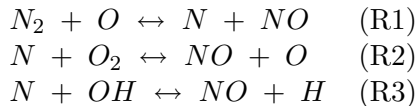
$$\langle \Xi_k | \Psi \rangle = \left\langle \frac{\partial}{\partial x_j} \left(D_k \frac{\partial Y_k}{\partial x_j} \right) \middle| \Psi \right\rangle, \quad (15)$$

In fact Ξ can not be obtained from this equation because it is not possible to calculate the concentration gradients at small scales. Therefore the simple IEM model (Interaction by Exchange with the Mean) [23], which is also viewed as the LMSE model (Linear Mean Square Estimation) [24], is used to estimate Ξ so that

$$\Xi = \frac{\varepsilon}{k} \frac{\tilde{\mathbf{Y}} - \mathbf{Y}}{C} \quad (16)$$

The non dimensional constant C has been determined from numerical experiments [25] which lead to an optimal value of 0.7.

The vector $\underline{\omega}$ is obtained from a simplified chemical mechanism of 41 species and 120 reactions which involve carbonated species only to C4. Heavier fuel species are assumed to undergo cracking during vaporization. NOx formation in the combustor is assumed to result mainly from the Zeldovich thermal NO mechanism according to



The temperature dependent part k_T of each forward reaction rate can be written in the form

$$k_T = A T^b \exp\left(\frac{E_a}{RT}\right). \quad (17)$$

The pre-exponential factor A , the exponent b and the activation energy are given in table 1.

3 The calculation conditions

3.1 Geometry and calculation grid

A picture of the calculated combustion chamber is given Fig. 1. The multi-point fuel injector can be seen from the lateral window which is used for the experimental visualizations. As shown by Fig. 1, the injection device has an axial symmetry but the chamber has a square cross section. To shorten the calculation time the combustion chamber downstream of the injector is modelled by a cylindrical duct with a cross area equal to that of the real chamber. Therefore the calculations are achieved in a 2D geometry with an axial symmetry. The cross area of the combustor is constant just after the injector then decreasing until the outlet section as shown by Fig. 2 which gives the calculation grid. Because of the small size of the meshes, the refinement of the calculation grid around the injector must be seen on the right part of the figure. The arrows referenced by **injairI**

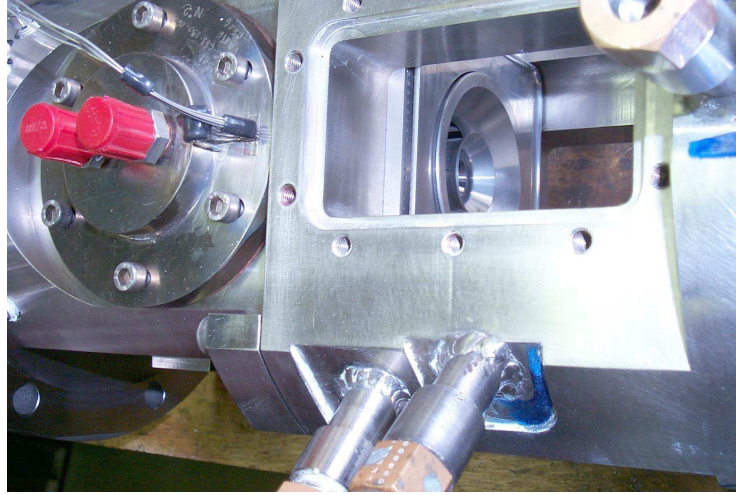


Figure 1: Combustion chamber with multi-point injector

with $\mathbf{I} = 1, 4$ indicate the air inlets in the experimental device. The arrows referenced by \mathbf{injkI} with $\mathbf{I} = 1, 2$ indicate the liquid fuel inlets. The inlet $\mathbf{injk1}$ corresponds to the pilot injection and the inlet $\mathbf{injk2}$ corresponds to the multi-point injection.

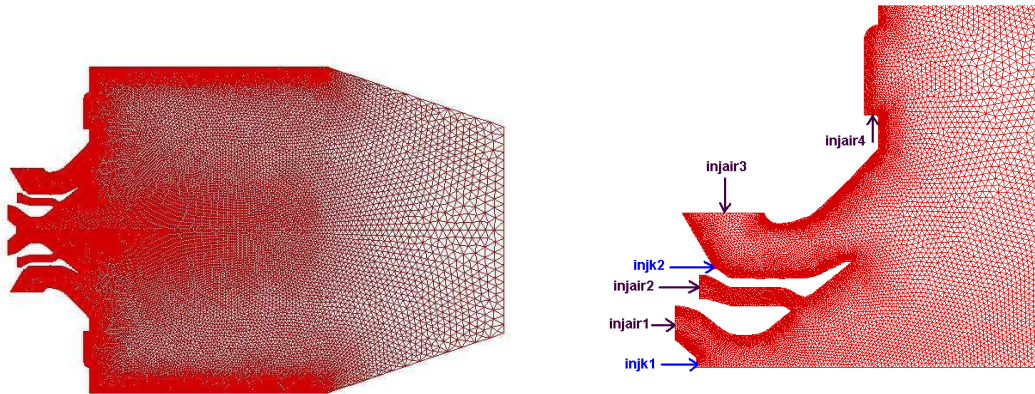


Figure 2: The calculation grid of the multi-point combustor: general view (left) and detail of the injector zone (right)

3.2 The boundary conditions

The results presented in this paper correspond to the two operating points summarized in table 2. The air flow rates are imposed on surfaces corresponding to the inlets referenced from $\mathbf{injair1}$ to $\mathbf{injair4}$. The pressure is imposed in the outlet section. It is well known that the vaporization rate of the fuel droplets has a large influence on the combustion process and therefore on the physics of the reactive flow. This rate is influenced by the size of the droplets which results on one hand from the initial conditions and on the other hand from the physical phenomena involving these droplets. Some numerical experiment have shown that, in absence of secondary break up model, the initial droplet size distribution has a drastic influence on the vaporization rate. However, when the secondary break up model is used, the influence of the initial droplet size distribution

	pressure (bar)	air inlet temperature (K)	air flow rate (kg/s)	fuel flow rate (g/s)	combustor equivalence ratio
idle conditions	4	470	0.344	5.03 100 % pilot	0.215
take off conditions	19	728	1.295	38.17 15 % pilot 85 % multi-point	0.433

Table 2: Operating conditions

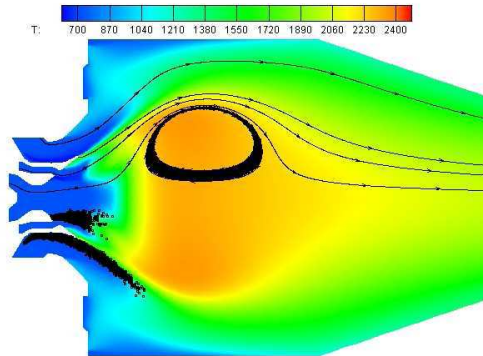


Figure 3: Typical results: temperature field, streamlines (upper part) and trajectories of the droplets issuing from the pilot and multi-point injectors (lower part)

is strongly reduced because the biggest droplets very rapidly break up until the droplet Weber number goes under its critical value. In the considered multi-point injector the initial droplet size distribution is not well known because the characterization of this injector at high pressure is very difficult. However the droplets are injected with a Weber number higher than the critical value and thus undergo secondary break up. The secondary break up model had to be used so that a very accurate initial droplet size distribution was not required. In the simulations all the droplets are injected with an initial diameter of $30 \mu\text{m}$ and an initial temperature of 300 K . For the multi-point injection no velocity slipping with the gas was introduced because numerical experiments did not evidence any influence of a velocity slipping. For the droplets issuing from the pilot injector the initial velocity components were 5 m/s both according to x and r . The droplets running into the wall undergo inelastic rebound and thermal exchange with the wall.

4 The numerical results

4.1 The main features of the reactive flow

Before going to the detailed results, it is necessary to point out the main features of the flow which can be drawn from Fig. 3. The organization of the flow is mainly influenced by the swirl imposed to the injected air. The effect of this swirl is to deflect the streamlines to the external walls and thus to create a recirculation zone around the axis of the combustor, as shown in the upper part of Fig. 3. This recirculation receives all the fuel of the pilot injector and a part of the fuel of the multi-point injector. The conjunction of a locally high FAR and a long residence time leads to a very high temperature in this recirculation. The droplets issuing from the pilot injector

with an angle of approximately 30° with the axis hit the wall, then enter in the recirculation zone and suddenly evaporate and disappear. In Fig. 3, they are represented only from the point where they leave the wall after inelastic rebound. The droplets issuing from the multi-point injector are going along the border of the recirculation and evaporate more progressively. The combustion starts between the two droplets streams just after the internal multi-point injector. Some

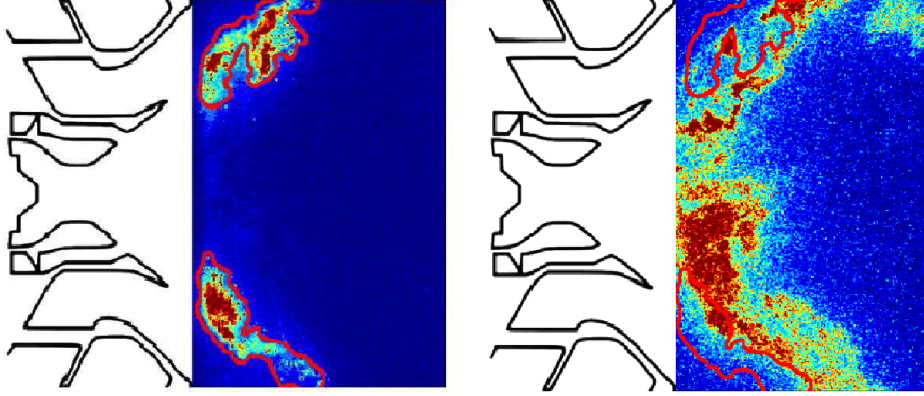


Figure 4: Instantaneous PLIF visualizations of the vaporized fuel (left) and OH radical (right) in idle operating conditions

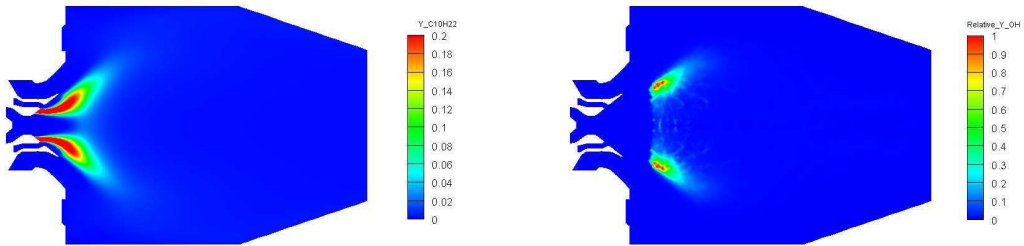


Figure 5: Calculated concentrations obtained in idle operating conditions: mass fraction of the vaporized fuel (left) and relative concentration of the OH radical (right)

PLIF visualizations have been achieved in different conditions of pressure and inlet temperature. Visualizations of the vaporized fuel and the OH radical could be obtained simultaneously. Fig. 4 presents such visualizations obtained in idle conditions, where the fuel is injected through the pilot injector in the shape of a widely open cone. This figure shows that the vaporized fuel lies on the downstream part of the injection cone and that the reaction zone indicated by the presence of the OH radical is located on the inner side of this cone. Fig. 5 gives the mass fraction of the vaporized fuel and the relative concentration of the OH radical obtained numerically in the idle operating conditions. For both species, the location of the high concentration zones are similar in the experiment and in the simulation but, in the experiment, the cone is more widely open and the OH radical has a higher concentration close to the injector. It is possible that, in the simulation, the rebound on the wall is treated with a too large elasticity which results in a too small cone angle for the fuel.

4.2 Influence of the swirl intensity

In order to optimize the combustor, different values of the azimuthal velocity component of the air entering through the external swirler have been tested keeping constant all the other

parameters. The changes of this velocity component result in different values of the angle between the inlet velocity vector and the vector obtained by subtraction of the azimuthal component. These values are equal to 30° , 40° , 50° and 60° respectively. Fig. 6 gives the temperature fields obtained for these different angles in the idle conditions. It can be noticed that the larger the

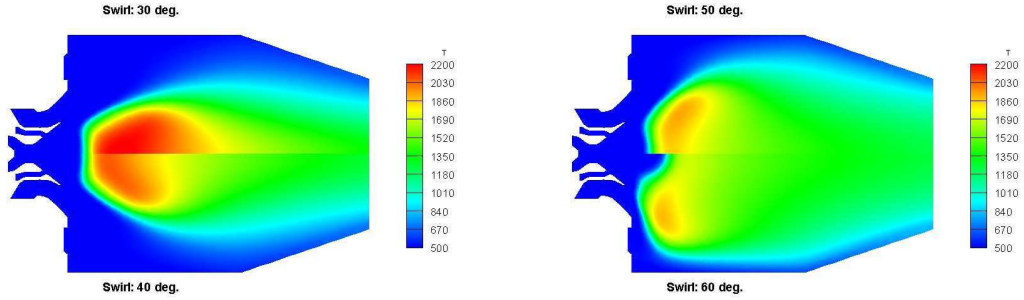


Figure 6: Temperature field obtained in idle conditions for different swirl angles: 30° , 40° on the left, 50° , 60° on the right

angle the more extended the zone of high temperature (the zone where T is larger than 1000 K). The explanation is that a larger angle results in a larger recirculation zone around the axis and that the burning gases are located in this recirculation zone and in its near surroundings. On the other hand the maximum of temperature is lower when the recirculation is very extended because the mixing is more intense in large recirculation zones so that the FAR is more homogeneous. Fig.

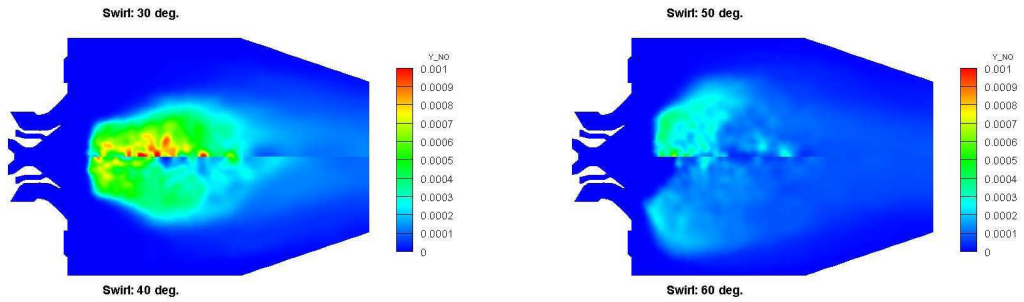


Figure 7: NO mass fraction field obtained in idle conditions for different swirl angles: 30° , 40° on the left, 50° , 60° on the right

7 gives the NO mass fraction fields obtained for the different swirl angles in the idle conditions from the lagrangian treatment described in Sec. 2.3. Since a minimum level of temperature of about 1800 K is required for the thermal NO formation, the highest NO mass fraction appears for the smallest angle of 30° which gives rise to the highest maximum of temperature. When the angle increases, the extension of the zone with temperatures higher than 1000 K becomes larger but the zone with temperatures above 1800 K is smaller. The NO emission index in g of emitted NO per kg of injected fuel decreases with the swirl angle as well, as can be seen in Fig. 10. Fig. 8 gives the temperature fields obtained for the different swirl angles in the take off conditions. the same behavior as in idle conditions can be noticed: The extension of the zone with temperatures higher than 1200 K increases with the swirl angle but, unlike the previous case, the zone with temperatures higher than 1800 K remains rather large for all the angles. Fig. 9 gives the NO mass fraction fields obtained for the different swirl angles in the take off conditions. The angle of 50° gives rise to the highest NO mass fraction peak and to an extended zone of high NO mass fraction. However, as shown in Fig. 10, the maximum of NO emission index is obtained for the angle of 40° . The reason is that for this angle the zone of high NO mass fraction is not limited to the axial recirculation zone and extends until the outlet section.

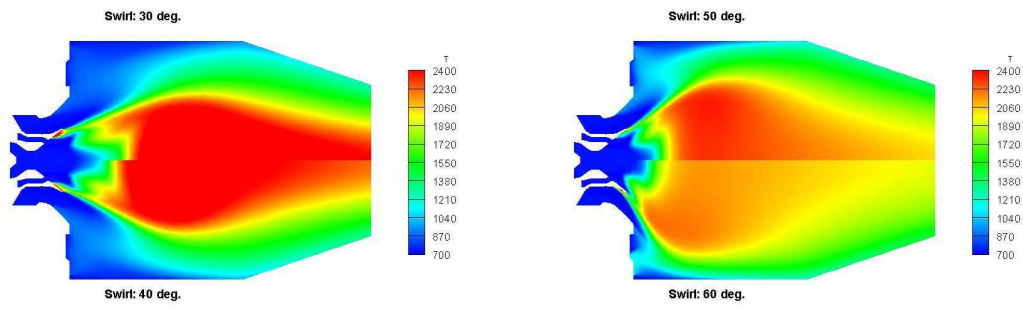


Figure 8: Temperature field obtained in take off conditions for different swirl angles: 30°, 40° on the left, 50°, 60° on the right

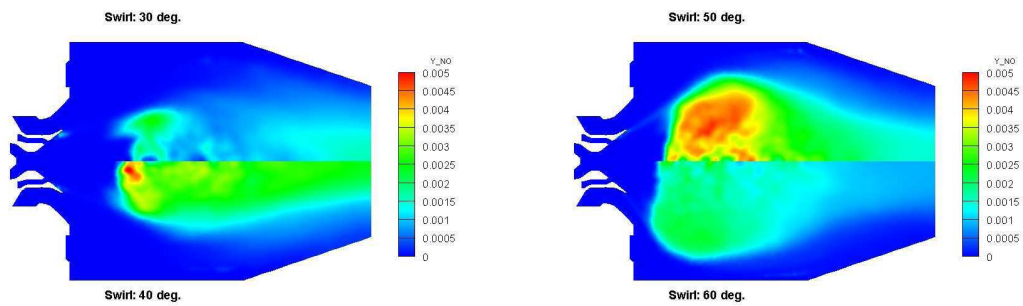


Figure 9: NO mass fraction field obtained in take off conditions for different swirl angles: 30°, 40° on the left, 50°, 60° on the right

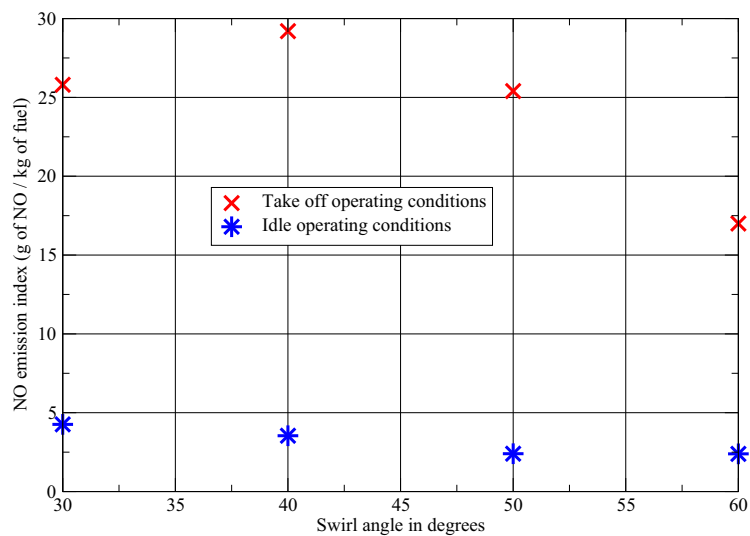


Figure 10: NO emission index versus swirl angle for idle and take off operating conditions

Some measurements of the NO emission index gave the values of 0.8 g/kg at idle and 12.6 g/kg at take off operating conditions. These values have to be compared to the values obtained numerically for a swirl angle of 50° , i. e. 2.4 g/kg and 25.4 g/kg respectively. The most probable reason for the emission index overestimation by the numerical simulation is that the radiative transfer were not taken into account in the energy balance. For these radiative transfer can lead to a temperature decrease of 50 K to 100 K in the hot zones of the reactive flow and thus to a decrease of the NO emission rate by a factor 2 to 3.

5 Conclusion

In order to minimize the NOx emission index of the aircraft engines, gas turbine combustors including a multi-point injection device are designed. The optimization of these combustors requires CFD numerical simulations. The corresponding numerical tools have been presented. They include a lagrangian treatment of the gas phase which is well adapted to account for the turbulence-chemistry interaction and from which the NO mass fraction field in the combustor can be deduced. Some axisymmetric calculations have been achieved to study the influence of a geometrical parameter on the NO emission index. This parameter which can not be easily changed in the combustor experimentally tested is the inlet swirl angle, a quantity which is related to the swirl intensity of the main inlet flow. For the take off conditions the maximum value of the NO emission index results from the competition of two opposed phenomena: on one hand the increase of the swirl intensity tends to enlarge the recirculation zone where burnt gases are located, on the other hand it tends to improve the mixing and thus to decrease the extension of the high FAR zones and to reduce the temperature peaks. Note that in the next future some experimental work will be done in the framework of the French national programme TOSCA to assess the validity of the trend deduced from these calculations.

The numerical simulations seem to overestimate the NO emission index. In a further work, the radiative transfer will be taken into account in order to correct the temperature field and thus to calculate more accurately the NO concentration field.

References

- [1] W. Dodds. Engine and aircraft technologies to reduce emissions. *UC Technology Transfer Symposium "Dreams of Flight"*, San Diego, March 1 2002.
- [2] C. Guin and P. Trichet. Optimisation of a two-head lean prevaporised premixed combustor. *Aerospace Science and Technology*, 8:35,46, 2004.
- [3] H. C. Mongia. Perspective of combustion modeling for gas turbine combustors. *AIAA Paper*, 2004-0156.
- [4] C. Guin. Caractérisation des systèmes d'injection prémélangés en auto-inflammation et remontée de flamme. *AVT Symposium on Gas Turbine Engine Combustion, Emissions and Alternative Fuels*, Lisbonne, 12-16 Octobre 1998.
- [5] D. Galley, A. Pubill Melsió, S. Ducruix, F. Lacas, D. Veynante, Y. Sommerer, and T. Poinsot. Dynamics of lean premixed systems: Measurements for large eddy simulation. In *Proceedings of the ERCOFTAC International Symposium on Engineering Turbulence Modelling and Measurements - ETMM6 - Sardinia, Italy*.

- [6] H. Kaaling, R. Rydén, Bouchié Y., Ansart D., P. Magre, and C. Guin. RQL combustor development including design, CFD calculations, CARS measurements and combustion tests. *13th international symposium on air breathing engines (ISABE), Chattanooga, TN (USA), ONERA-TAP-97-140*.
- [7] D. L. Straub, K. H. Casleton, R. E. Lewis, T. G. Sidwell, D. J. Maloney, and G. A. Richards. Assessment of rich-burn, quick-mix, lean-burn trapped vortex combustor for stationary gas turbines. *Journal of Engineering for Gas Turbines and Power*, 27:36–41, 2005.
- [8] W. Dodds. Twin annular premixing swirler (TAPS) combustor. *The Roaring 20th Aviation Noise and Air Quality Symposium, University of California, Berkeley*, March 2 2005.
- [9] S. D. Stouffer, D. R. Ballal, J. Zelina, D. T. Shouse, R. D. Hancock, and H. C. Mongia. Development and combustion performance of a high-pressure WSR and TAPS combustor. *43rd AIAA Aerospace Sciences Meeting and Exhibit, AIAA Paper*, 2005-1416, 10-13 January 2005.
- [10] B. Zamuner, P. Gilbank, D. Bissières, and C. Bérat. Numerical simulation of the reactive two-phase flow in a kerosene/air tubular combustor. *Aerospace Science and Technology*, 6:521–529, 2002.
- [11] Ha J. and Zhu Z. Computation of turbulent reactive flows in industrial burners. *Applied Mathematical Modelling*, 22:1059–1070, 1998.
- [12] F. Grinstein and C. Fureby. Les studies of the flow in a swirl gas combustor. In *Proceedings of the Combustion Institute*, volume 30, pages 1791–1798, 2005.
- [13] T. Kobayashi. Large eddy simulation for engineering applications. *Fluid Dynamics Research*, 38:84–107, 2006.
- [14] A. X. Sengissen, J. F. Van Kampen, R. A. Huls, G. G. M. Stoffels, J. B. W. Kok, and T. Poinsot. LES and experimental studies of cold and reacting flow in a swirled partially premixed burner with and without fuel modulation. *Combustion and Flame*, 150:40–53, 2007.
- [15] P. Caillau and F. Dupoirieux. Calculs d’écoulements turbulents réactifs dans les foyers aéronautiques. In *AGARD Conference Proceedings, Symposium on Heat Transfer and Cooling in Gas Turbines, Antalya (Turquie)*, volume 527, Octobre 1992.
- [16] R. Borghi, F. Dupoirieux, B. Zamuner, F. Galzin, and T. Mantel. Recent progress in the modelling of turbulent combustng flows. In *Proceedings of the 4th World Conference on Experimental Heat Transfer, Fluid Mechanics and Thermodynamics, Brussels (Belgium)*, 2-6 June 1997.
- [17] A. K. Tolpadi, S. M. Correa, D. L. Burrus, and Mongia H. C. Monte Carlo probability density function method for gas turbine combustor flowfield predictions. *Journal of Propulsion and Power*, 13, Number 2:218–225, 1997.
- [18] H. W. Ge and E. Gutheil. Simulation of a turbulent spray flame using coupled PDF gas phase and spray flamelet modelling. *Combustion and Flame*, 153:173–185, 2008.
- [19] F. Grisch, M. Orain, B. Rossow, E. Jourdanneau, and Guin C. Simultaneous equivalence ratio and flame structure measurements in multipoint injector using plif. *AIAA Paper*, 2008-4868.
- [20] B. Zamuner and F. Dupoirieux. Numerical simulation of soot formation in a turbulent flame with a monte carlo pdf approach and detailed chemistry. *Combustion Science and Technology*, 158:407–438, 2000.

- [21] B. F. Magnussen and B. H. Hjertager. On mathematical modeling of turbulent combustion with special emphasis on soot formation and combustion. In *Sixteenth Symposium (International) on Combustion*, pages 719–729. The Combustion Institute, 1977.
- [22] P. Chevalier, B. Courbet, D. Dutoya, P. Klotz, E. Ruiz, J. Troyes, and P. Villedieu. CEDRE: development and validation of a multiphysic computational software. *1st European Conference for Aerospace Sciences (EUCASS), Moscou, Russie*, 2005.
- [23] C. Aubry and Villiermaux J. Representation d’un mélange de deux courants de ractifs dans un racteur agit continu. *Chemical Engineering Science*, 30:457–464, 1975.
- [24] C. Dopazo and O’Brien E. An approach to the autoignition of a turbulent mixture. *Acta Astronautica*, 1:1239–1266, 1974.
- [25] B. Zamuner and R. Borghi. Influence of physical phenomena on the formation of pollutants in combustion. In *Pollutants from Combustion, C. Vovelle (Ed.)*, pages 51–73, 2000.